

Correlation between normal and superconducting states within the Fermi-liquid region of the T - p phase diagram of quantum-critical heavy-Fermion superconductors

M. ElMassalami,^{1,*} P. B. Castro,^{1,†} and M. B. Silva Neto^{1,‡}

¹*Instituto de Física, Universidade Federal do Rio de Janeiro,
Caixa Postal 68528, 21941-972 Rio de Janeiro RJ, Brazil*

Extensively reported experimental observations indicate that on varying pressure (p) within the T - p phase diagram of most quantum critical heavy fermion (HF) superconductors, one identifies a cascade of distinct electronic states which may be magnetic, of Kondo-type, non-conventional superconducting, Fermi Liquid (FL), or non-FL character. Of particular interest to this work is the part of the phase diagram lying below a specific phase boundary, $T_{\text{FL}}^*(p^*)$, across which the transport and thermodynamic properties switch over from non-FL into FL behavior. Remarkably, this nontrivial manifestation of FL phase is accompanied by (i) the characteristic $\rho_o + AT^2$ dependence ($\rho_o =$ residual resistivity), (ii) a superconductivity below $T_c \leq T_{\text{FL}}^*(p^*)$, and (iii) a universal scaling of T_c and A : $\ln \frac{T_c}{\theta} \propto A^{-\frac{1}{2}}$ ($\theta =$ characteristic energy scale). We consider that such features are driven by a fluctuation-mediated electron-electron scattering channel with the mediating quasiparticles being either spin fluctuations [Mathur *et al.* Nature 394, 39 (1998)] or valence fluctuations [Miyake and Watanabe, Phil. Mag.97, 3495–3516 (2017)] depending on the character of the neighboring instability. On adopting such a scattering channel and applying standard theories of Migdal-Eliashberg (superconductivity) and Boltzmann (transport), we derive analytic expressions that satisfactorily reproduce the aforementioned empirical correlations in these heavy fermion superconductors.

I. Introduction

There is ongoing interest in investigating the correlations between the normal-state and superconducting properties of heavy fermion (HF) superconductors when subjected to a variation in a nonthermal control parameter such as pressure p , concentration of charge carriers n , stoichiometry/doping x , disorder, or magnetic field H .^{1–5} Driven by ease and convenience, the evolution of these correlations is often investigated within a T - p phase diagram; there, an extrapolation of the phase boundaries down to zero temperature often leads to one or two quantum critical/crossover points.^{1–7} One is usually attributed to a magnetic instability at p_m ; often, it is accompanied by a superconducting dome wherein the superconductivity is considered to be driven by spin fluctuations.⁶ The other point, at p_v , is usually assigned to a valence instability⁷ which, as well, is often accompanied by a superconducting dome with the superconductivity considered to be driven by valence fluctuations.^{7,8}

A surge of superconducting dome within the neighborhood of a magnetic quantum critical point is also manifested in other superconducting family, such as high- T_c cuprates and Fe-based pnictides and chalcogenides.^{9,10} Much of the understanding of the superconducting and normal-state properties were obtained from theoretical and experimental investigation of three regions of the dome: the two neighboring the emergence and disappearance of the superconductivity (at the left and right $T_c \rightarrow 0$) while the third is at the middle wherein T_c is a maximum. Analysis of the character of the left and middle regions is usually complicated by the additional influence of competing antiferromagnetic, spin glass, charge and stripes, or pseudogap phases. In contrast, investigation of the region at the right $T_c \rightarrow 0$ limit is much

simpler since only two states are involved, namely the superconducting and the FL phases.^{11–15} This work, in line with Refs. 11–15, investigate the evolution of (and correlation among) the superconducting and normal states within the FL region of the HF T - p phase diagram. As shown below, in contrast to these references, (i) we consider explicitly the normal-state FL character, (ii) we do not invoke any additional impurity scattering; rather we consider the spin-fluctuations to be operating within patches of the sample (the average dimension of a patch is longer than the mean free path and coherent length while their concentration is reflected in the excess residual resistivity), and most importantly (iii) we consider that the very same fluctuation-mediated electron-electron scattering channel is responsible for the evolution of both the superconductivity and the FL character.

It is worth recalling that various experiments reveal the presence of phase-boundary curve, e.g. $T_{\text{FL}}^*(p^*)$ within the HF T - p phase diagram, across which both the transport and thermodynamic properties switch over from non-Fermi-liquid (NFL) into a Fermi-liquid (FL) behavior. Such a switch is best illustrated by the electronic contribution to the low-temperature resistivity, $\rho(T, p)$, of typical HF superconductors: Within the NFL phase,

$$\rho(T > T_{\text{FL}}^*[p^*], p \leq p^*) - \rho_x = \rho_o + A_{\text{NFL}} T^n, \quad [n < 2], \quad (1)$$

while within the FL phase,

$$\rho(T_c < T < T_{\text{FL}}^*[p^*], p > p^*) - \rho_x = \rho_o + AT^2, \quad (2)$$

where $\rho_x = \rho_o^{\text{n.f.}} + \rho_{\text{n.f.}}(T)$ represents all non-fluctuation-related (e.g. defects, phonon, magnetic) contributions (see end of Subsec. II A). Within the FL region (which starts at the switching of NFL into FL character and

ends when $T_c \rightarrow 0$), we denote the excess contribution of the residual resistivity by ρ_o , that of the *quadratic-in-T* coefficient by A , and that of the superconductivity transition by T_c ; all these contributions are attributed to a fluctuation-mediated electron-electron (e-e) scattering channel (see below). Generally, these $\rho_o(p)$, $A(p)$, and $T_c(p)$ parameters — derived from experimental $\rho(T, p)$ curves — manifest a dramatic and non-monotonic variation around each of the critical p_m and p_v points (see, e.g., Figs. 2,3,4).

In this work, we are interested in analyzing and rationalizing the baric evolution of $\rho_o(p)$, $A(p)$, and $T_c(p)$ within the FL region of various archetype HF superconductors. Our analysis identified two universal correlations among these ρ_o , A , and T_c parameters. We argue that the fluctuation-mediated electron-electron scattering channel is responsible for the emergence of the superconductivity, the FL character and the correlations among them.

The text below is organized as follows. We first recall some helpful insight regarding the fluctuation-mediated e-e scattering process.^{6,7} In Subsec. II B we extract, identify, and generalize two main empirical correlations. In Subsec. II C we argue that these correlations are driven by a fluctuation-mediated e-e interaction channel. Such fluctuations can be either spin fluctuation⁶ or valence fluctuation⁷ (generically referred to as fluctuation). Although we consider below the spin-fluctuation exchange mechanism⁶, generalization to valence fluctuation⁷ is implicitly assumed. On adopting such a mechanism and applying standard Migdal-Eliashberg description of superconductivity and Boltzmann's transport theory, we derive analytic expressions that compare favorably with the empirically-obtained correlations. Comparison to other fluctuation-bearing/defect-bearing superconductors will be briefly discussed in Sec. III; there, we demonstrate the generality of our approach by discussing the Kadowaki-Woods and gap-to- T_c ratios of these HF superconductors.

II. Analysis

A. Some Preliminaries on the fluctuation-mediated e-e interaction channel

It is recalled that a typical T - p phase diagram of most quantum-critical HF superconductors exhibits a series of distinct electronic states (see, e.g., Figs. 2(a)-3(a) and Refs. [3, 8, and 16]). Often, the initial state is an antiferromagnetic, represented in Fig. 1(a) as simple two-dimension Neel-type arrangement. Beyond a critical value of the control parameter, p_m in the present cases, the localized moments and the three-dimensional magnetic structure are quenched leading to a series of "nonmagnetic" states which can be of Kondo-type, non-conventional superconducting, non-FL, or FL character. Nevertheless, some remnant magnetic fluctuations persist

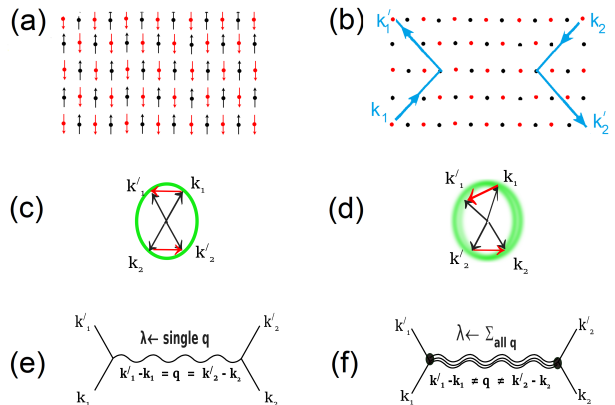


FIG. 1. A sketch of a fluctuation-mediated e-e interaction channel. (a) An antiferromagnet structure representing an initial state in the phase diagram of a typical heavy fermion superconductor. The tiny arrows denote localized magnetic moments of atomic entities (represented by the small solid circles). (b) The nonmagnetic state after the quench of localized magnetic moments and, consequently, the magnetic structure. Within the direct lattice, the two electrons with \mathbf{k}_1 and \mathbf{k}_2 scatter into final states \mathbf{k}'_1 and \mathbf{k}'_2 . (c) A $\delta\mathbf{g} = \mathbf{0}$ two-electrons scattering process in the reciprocal space: As that $\mathbf{q} = \mathbf{k}'_1 - \mathbf{k}_1 - \mathbf{g}$, the phase space for scattering is quite limited; a Fermi-liquid state is possible only at very low temperatures. (d) The $\delta\mathbf{g} \neq \mathbf{0}$ two-electrons scattering process in the reciprocal space: as that $\mathbf{q} = \mathbf{k}'_1 - \mathbf{k}_1 - \mathbf{g} - \delta\mathbf{g}$, the phase space available for scattering is considerably enlarged, leading to a robust superconducting and Fermi-liquid states. (e) Feynman diagram of the $\delta\mathbf{g} = \mathbf{0}$ process [as in panel (c)] wherein only longitudinal modes are involved. (f) The Feynman diagram of the $\delta\mathbf{g} \neq \mathbf{0}$ process [as in panel (d)] which is mediated by exchanging all kinematically unconstrained modes.

within various micro-sized patches which are distributed randomly within an otherwise metallic matrix.¹⁷

These magnetic fluctuations are considered to mediate an e-e scattering process⁶: as shown in Figs. 1(b-f), the two electrons with \mathbf{k}_1 and \mathbf{k}_2 scatter into final states \mathbf{k}'_1 and \mathbf{k}'_2 . In particular, the electron, initially at a state \mathbf{k}_1 , goes into a final state \mathbf{k}'_1 after being scattered by a mode with wavevector \mathbf{q} ; in doing so, it transfers an amount of energy and quasi-momentum satisfying $\mathbf{k}'_1 - \mathbf{k}_1 - \mathbf{q} = \mathbf{g} + \delta\mathbf{g}$ where \mathbf{g} is a vector in a reciprocal magnetic lattice while $\delta\mathbf{g}$ is an uncertainty in \mathbf{g} due to the inherent nature of the process leading to fluctuation (most obvious for the doping process).

We consider that, within the Fermi-liquid state of these HF superconductors, an increase in pressure leads to a reduction of the size and density of the fluctuation-bearing patches,¹⁷ till eventually one reaches, at very high pressure, the fluctuation-free state wherein no modes are available for mediation. This, as will be detailed below in Figs. 2, 3, and 4, leads to a complete removal of fluctuation-related features, namely the superconductivity ($T_c \rightarrow 0$), the Fermi-liquid state ($A \rightarrow A_o$), the residual resistivity ($\rho \rightarrow \rho_o$), and their correlations.

Let us now discuss the fluctuation-based mediation

within the FL region. First, we consider the case satisfying $\delta\mathbf{g} = \mathbf{0}$ condition of Figs. 1(c) and 1(e). Here, the quasi-momentum $\mathbf{q} = \mathbf{k}'_1 - \mathbf{k}_1 - \mathbf{g}$ is conserved exactly. Accordingly, only longitudinal modes with a well defined polarization, $\hat{\mathbf{e}}(\mathbf{q} = \mathbf{k}'_1 - \mathbf{k}_1)$, will be involved. This means that the phase space available for momentum relaxation will be quite limited leading to, if any, a very small T_c and A .

Secondly, in contrast to above, the surge of fluctuation-based mediation satisfying $\delta\mathbf{g} \neq \mathbf{0}$ condition, Figs. 1(d) and 1(f), provides a source for short wavelength (large \mathbf{q}) phase interference. This $\delta\mathbf{g} \neq \mathbf{0}$ condition implies that the quasi-momentum $\mathbf{q} = \mathbf{k}'_1 - \mathbf{k}_1 - \mathbf{g} - \delta\mathbf{g}$ is no longer conserved since $\delta\mathbf{g}$ is arbitrary.¹⁸⁻²⁰ Then, multiple modes [longitudinal and transverse, of all polarizations $\hat{\mathbf{e}}(\mathbf{q} \neq \mathbf{k}'_1 - \mathbf{k}_1 - \mathbf{g})$] become kinematically available, Fig. 1(f). As shown in Fig. 1(d), the phase space available for momentum relaxation is considerably enlarged: this leads to an enhanced T_c and A .

Considering the above partitioning of a fluctuation-bearing sample into two spacial regions, Matthiessen's rule suggests a sum of two types of contributions: (i) one type is related to normal (non-fluctuation-bearing) patches; these are the residual resistivity ρ_o° , the coefficient A_o , the coupling constant λ_o , and the mean free path ℓ_o ($\ell_o \propto \frac{1}{\rho_o^\circ}$). (ii) The other type is related to fluctuation-bearing patches within which, we consider, a fluctuation-mediated e-e scattering channel is operating and as such leading to excess contributions denoted as A , λ , ℓ , and ρ_o . Below we consider ρ_o to be arising from those patches and as such it measures the strength of the fluctuation-related channel while ρ_o° as a measure of all normal processes.

The total contribution is denoted as ρ_o^{tot} , A_{tot} , λ_{tot} , or ℓ_{tot} . Often, the non-fluctuation-bearing ρ_o° and A_o contributions are obtained by extrapolation. In our case here, these values (shown as large green circle in Figs. 2, 3, and 4 and tabulated in Table I) were estimated from the very-high-pressure region whereat $T_c \rightarrow 0$, indicating, we assume, the quench of the fluctuations. Then each excess, fluctuation-related contribution $X = X_{\text{tot}} - X_o$, is obtained from²¹

$$\rho_o = \rho_o^{\text{tot}} - \rho_o^\circ, \quad (3a)$$

$$A = A_{\text{tot}} - A_o, \quad (3b)$$

$$\lambda = \lambda_{\text{tot}} - \lambda_o, \quad (3c)$$

$$\ell = 1/\left(\frac{1}{\ell_{\text{tot}}} - \frac{1}{\ell_o}\right). \quad (3d)$$

For theoretical analysis, it is more convenient to measure the strength of the fluctuation-related scattering channel via the effective mean free path, the *scaling length* $\ell \propto 1/\rho_o$. Then any variation in the control parameter (e.g. pressure, alloying, or defect incorporation²²) would be reflected in ℓ and manifested as a variation in the superconductivity, the FL character, and the correlation among $\rho_o(\ell)$, $T_c(\ell)$ and $A(\ell)$; within the FL region of Figs. 2-4, a pressure increase leads to a reduction of these

parameters indicating an increase in fluctuation-related ℓ . The functional dependence of ℓ on, e.g., pressure will not be discussed in this work.

B. Empirical analysis: extraction of correlations among ρ_o , A , and T_c

Below, we review the baric evolution of $\rho_o(p)$, $A(p)$, and $T_c(p)$ of three representative HF superconductors for which detailed resistivity curves $\rho_{\text{tot}}(T, p)$ (essentials for determining these ρ_o , A , and T_c parameters) were reported. Special attention will be directed towards identifying the correlations.

1. CeCu₂X₂ (X=Si, Ge)

The T - p phase diagram and the baric evolution of T_c , A_{tot} , and ρ_o^{tot} of CeCu₂Ge₂ are shown in Figs. 2(a)-2(d) (Refs. 3 and 27) while those of CeCu₂Si₂ in Figs. 3(a)-3(d) (Refs. 4, 8, 26, 28, and 29). As evident, these plots highlight the dramatic baric evolution in particular around the critical points.

The phase diagram of each of CeCu₂X₂ manifests a FL character at sufficiently higher pressure; this is evidenced as a *quadratic-in-T* resistivity contribution, identified in Figs. 2(a) and 3(a) by the hatched area and the $n=2$ notation. At 20 GPa for CeCu₂Ge₂ and 7 GPa for CeCu₂Si₂, $T_c \rightarrow 0$; we identify this as a signal of a pressure-induced quench of the fluctuation-related FL contributions. Based on Eqs. 3, all parameters extrapolate to non-fluctuation-related contributions: $A \rightarrow A_o$ and $\rho_o \rightarrow \rho_o^\circ$ (see Figs. 2 and 3 and Table I).

Then for the purpose of empirical identification of any possible correlation *within the FL region*, we plot [$A_{\text{tot}}(p) - A_o$] versus [$\rho_o^{\text{tot}}(p) - \rho_o^\circ$] in Figs. 2(e) and 3(e), T_c versus [$\rho_o^{\text{tot}}(p) - \rho_o^\circ$] in Figs. 2(f) and 3(f), and $\ln[T_c(p)]$ versus $1/\sqrt{A_{\text{tot}}(p) - A_o}$ in Figs. 2(g) and 3(g).

Figures 2(e) and 3(e) show that within *the FL state, well above the critical pressures region*,^{1,2,25,26,30} one obtains

$$(A - A_o) \approx A_2(\rho_o - \rho_o^\circ)^2, \quad (4)$$

The A_o and A_2 parameter of each CeCu₂X₂ are given in Table I. It is noted that the absence of a linear-in- ρ_o term rules out any Koshino-Taylor contribution. On the other hand, Figs. 2(g) and 3(g) indicate that

$$\ln(T_c) \propto (A - A_o)^{-\frac{1}{2}}. \quad (5)$$

A closer look at Eqs. (4 and 5) suggests that a relation between T_c and $(\rho_o - \rho_o^\circ)$ can be derived; indeed the solid red curves in Figs. 2(f) and 3(f) were calculated based on Eq. 11 which is a derived equation (see Subsec. II C 3).

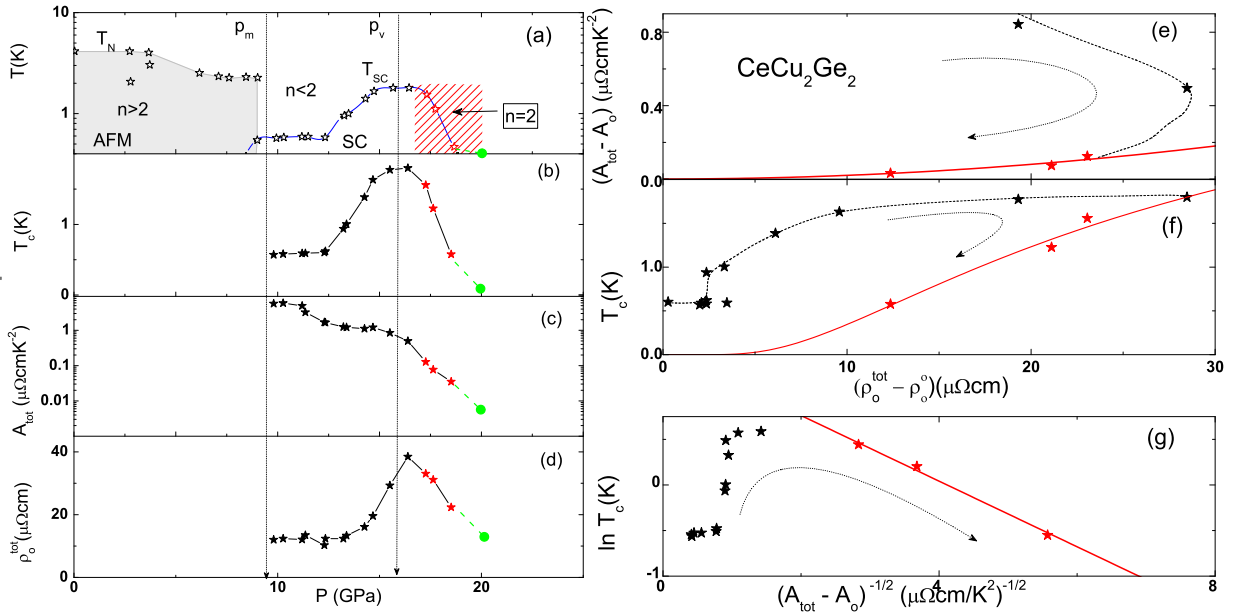


FIG. 2. T - p phase diagram and baric evolution of the parameters of CeCu_2Ge_2 (data taken from Ref. 3). (a) A semi-log T - p phase diagram showing the evolution of $T_N(p)$, $T_c(p)$, and the exponent $n(p)$. Vertical dashed arrows represent $p_m \approx 9.4$ GPa and $p_v \approx 16$ GPa.³ The dashed lines are visual guides while the curved arrows signal the direction of pressure increase. The red symbols and hatched area mark the FL region. Evolution of (b) $T_c(p)$, (c) $A_{\text{tot}}(p)$ in a semi-log plot, and (d) $\rho_o^{\text{tot}}(p)$. As discussed in text, for $p \rightarrow 20$ GPa, the pressure-induced strong reduction of the fluctuation leads to $T_c \rightarrow T_c^o \approx 0$, $A \rightarrow A_o$ and $\rho_o^{\text{tot}} \rightarrow \rho_o^o$: the limits at 20 GPa (large green circles) are shown in Table I. (e) Correlation of $[A_{\text{tot}}(p) - A_o]$ with $[\rho_o^{\text{tot}} - \rho_o^o]$. The solid line is a best fit to Eq. 9: A_0 and A_2 given in Table I. (f) T_c versus $[\rho_o - \rho_o^o]$: The solid line is calculated based on Eq. (11) of Subsec. II C 3. (g) $\ln(T_c)$ versus $(A_{\text{tot}} - A_o)^{-1/2}$. The solid red line is the best fit to linearized Eq. 10; θ and \mathcal{F} parameters are given in Table I.

TABLE I. Representative fit parameters of CeCu_2Ge_2 , CeCu_2Si_2 and CeCoIn_5 . Values of A_o and A_2 were obtained from a fit of Eq. 9 to Figs. 2(e), 3(e), 4(e): As $A_1 \approx 0$, it was fixed as $A_1 \equiv 0$. For all compounds, A_2 , θ and \mathcal{F} are close to each other, except A_2 of CeCoIn_5 which is orders of magnitude higher than the others: this together with the high value of T_c is most probably related to a relatively high strength of the fluctuation-related e-e scattering channel of CeCoIn_5 . It is worth noting that the strength and evolution of the fit parameters depend critically on the criteria for determining T_c (10-90%, 50%, onset, zero point etc.) and A (the sample geometry, which is often not precisely determined). Additionally, the widely different methods for sample synthesis and thermal treatment adopted by different groups give rise to a corresponding variation in sample-dependent properties. Although these non-fluctuation-related material properties are accounted for by T_o , A_o , and ρ_o^o , it is expected to lead to a wide scatter in the fit parameters. The scatter in the experimental curves leads to a large error value.

HF's	ρ_o^o	A_o	A_2	θ	\mathcal{F}
-	$\mu\Omega\text{cm}$	$\mu\Omega\text{cm}/\text{K}^2$	$\times 10^6 \Omega^{-1}\text{cm}^{-1}/\text{K}^2$	K	$\times 10^{-3} (\Omega\text{cm}/\text{K}^2)^{1/2}$
CeCu_2Ge_2	10(1)	$2.9(5) \times 10^{-3}$	$2.0(2) \times 10^{-4}$	4.4(2)	0.36(1)
CeCu_2Si_2	18.5(5)	0.010(5)	$7.0(5) \times 10^{-4}$	2.6(1)	0.49(1)
CeCoIn_5	0.130(5)	0.082(4)	6.0(2)	3.2(1)	0.18(1)

2. CeCoIn_5

The T - p phase diagram of CeCoIn_5 [Refs. 16, 31, 32, and 34] is shown in Fig. 4(a) while the baric evolution of $T_c(p)$, $A_{\text{tot}}(p)$ and $\rho_o^{\text{tot}}(p)$ are shown in Figs. 4(b), 4(c) and 4(d), respectively.

A comparison of the features of CeCoIn_5 with those of CeCu_2X_2 ($X=\text{Si}, \text{Ge}$) suggests an overall similarity in that:

- Figure 4(e) indicates that $A(p) - A_o$ is large but still *quadratic-in-* $[\rho_o(p) - \rho_o^o]$,
- Figure 4(f) reveals that the evolution of $T_c[\rho_o(p) - \rho_o^o]$ can be described by Eq. 11 (see Subsec. II C 3).
- Figure 4(g) shows that $\ln[T_c(p)]$ is linear in $[A(p) - A_o]^{-1/2}$.

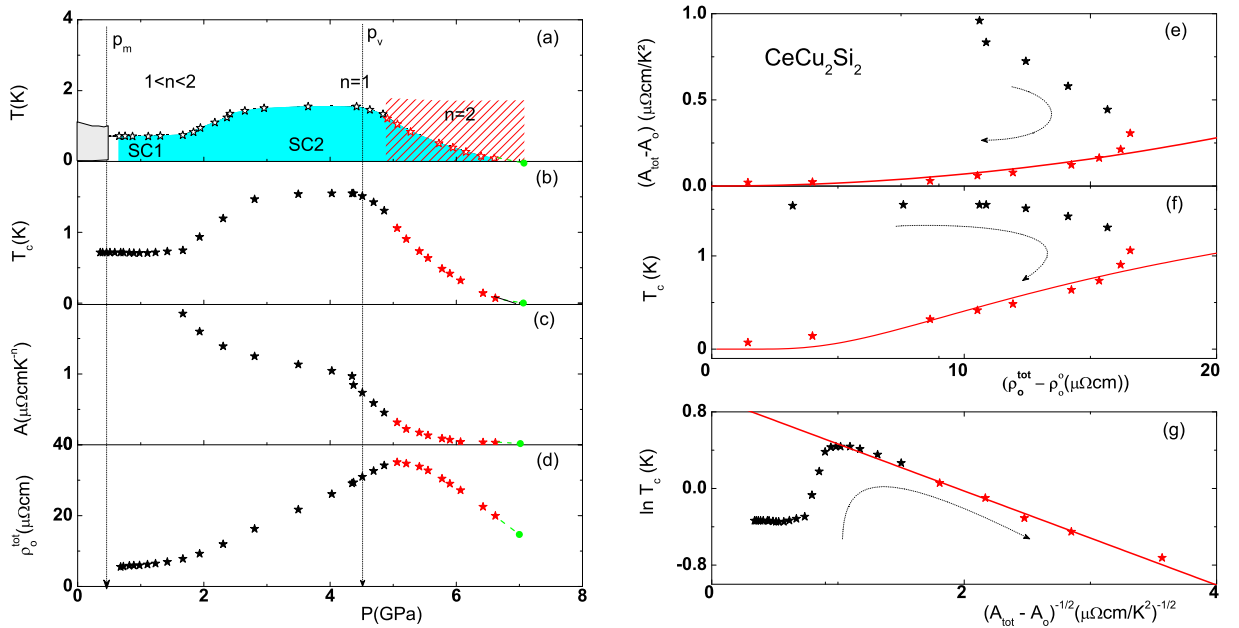


FIG. 3. (a) The T - p phase diagram and baric evolution of (b) $T_c(p)$, (c) $A_{\text{tot}}(p)$, and (d) $\rho_o^{\text{tot}}(p)$ of CeCu_2Si_2 . All curves were taken from the continuous line (the visual guide) of Ref. 8. For a discussion on the critical pressures p_m and p_v and the related superconductivity regions (SC 1 and SC II) see Ref. 8. The red symbols and hatched area mark the FL region while the dashed lines are visual guides. It is noted that, due to non-stoichiometry, defects, impurities or disorder, the reported parameters of CeCu_2Si_2 vary considerably from sample to sample; nonetheless, the overall evolution as well as the derived correlations are consistently similar.^{23–26} As $p \rightarrow 7$ GPa, $T_c \rightarrow 0$, $A \rightarrow A_o$ and $\rho_o \rightarrow \rho_o^o$ (see text): the extrapolation to 7 GPa (large green circles) are shown in Table I. (e) A plot of $[A(p) - A_o]$ versus $[\rho_o(p) - \rho_o^o]$. The best fit to Eq. 9 is shown as solid red curve; the fit parameters A_0 and A_2 are given in Table I. (f) T_c versus $[\rho_o(p) - \rho_o^o]$: For the solid calculated line, see Eq. (11) in Subsec. II C 3. (g) $\ln(T_c)$ versus $(A - A_o)^{-1/2}$. The straight red line is a best fit to linearization of Eq. (10): θ and \mathcal{F} are given in Table I.

C. Theoretical analysis: interpretation of the correlations among ρ_o , A , and T_c

The aforementioned experimental evidences emphasize that in spite of the wide differences in material properties of these HF superconductors, one observes: (i) A similarity in the overall evolution of the phase diagrams as well as in the baric evolution of their $T_c(p)$, $A(p)$, and $\rho_o(p)$. (ii) A nontrivial manifestation of neighboring superconductivity and FL phases. (iii) Two correlations (expressed in Eqs. 4 and 5) and a derived one; all manifested in Figs. 2,3,4. Below we discuss the significance of these features in terms of a fluctuation-mediated e-e scattering channel which, due to a modification in the kinematic constraints, is endowed with a significantly enlarged phase space for scattering, much larger than the traditional Baber or Umklapp e-e scattering channels.⁴⁷

Furthermore, the empirical analysis highlights the distinct and nontrivial contrast between the properties of the FL state of a HF superconductor and that of conventional weakly-correlated superconductor: It is remarkable that A is more than five orders of magnitude higher than the contribution expected for a typical Fermi-liquid metal ($A_o \simeq 10^{-7} \mu\Omega\text{cm}/\text{K}^2$).^{48–53}

Another contrast is that a conventional FL supercon-

ductor, in contrast to a HF one, does not manifest a correlation among ρ_o , T_c and A : ρ_o is determined by the electron-impurity scattering, $\rho_o \sim |V_{\text{imp}}|^2$; $T_c \sim e^{-1/\lambda}$ is associated with electron-phonon coupling, $\lambda \sim |V_{\text{ep}}|^2$; while A depends on e-e interaction, $A \sim |V_{\text{ee}}|^2$.

It is worth emphasizing that, although two exceptional cases were reported to yield a similar BCS-like correlation among T_c and A (see Ref. 54 and Subsec. II B), none of them manifest a correlation between A and ρ_o nor between T_c and ρ_o ; in fact, Anderson theorem excludes the latter relation. It is, then, quite puzzling that the aforementioned empirical analysis, see Figs. 2-4, delineate a distinct FL phase within which one identifies a surge of superconductivity and pressure-dependent correlations among ρ_o , A and T_c . This puzzle can be resolved if *the manifestation of superconductivity and FL state as well as the correlation of T_c (hallmark of superconductivity) and A (hallmark of normal FL state) are assumed to be driven by a retarded, spin-fluctuation⁶ or valence-fluctuation⁷ mediated e-e interaction*. This is reminiscent of the defect-induced, phonon-mediated e-e scattering in defectual-bearing systems (see Ref. 47)

The basic idea is discussed in Subsec. II A: within a HF superconducting sample, the fluctuation-related quasiparticles can be created or annihilated and that their me-

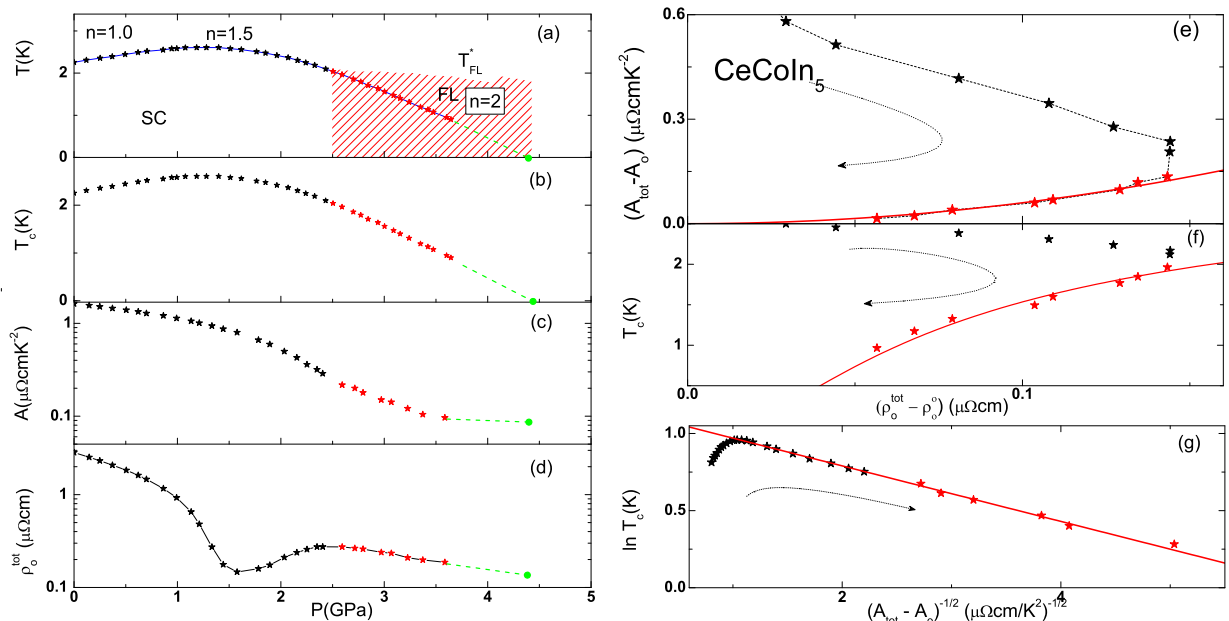


FIG. 4. (a) T - p phase diagram and baric evolution of (b) $T_c(p)$, (c) $A_{\text{tot}}(p)$, and (d) semilog plot of $\rho_o^{\text{tot}}(p)$ of CeCoIn_5 . All curves were taken from the continuous line (the visual guide) of Ref. 16. For more detail on this phase diagram, in particular, the position of critical p_m , see Refs. 16, 31–33. The red symbols and hatched area identify the FL region while the dashed lines are visual guides. For $p \rightarrow 4.4$ GPa, $T_c \rightarrow 0$, $A \rightarrow A_o$ and $\rho_o \rightarrow \rho_o^o$ (see text and Table I). (e) A plot of $A_{\text{tot}} - A_o$ versus $\rho_o^{\text{tot}} - \rho_o^o$. The solid curve is the best fit to Eq. 9 (see Table I). (f) T_c versus $(\rho_o^{\text{tot}} - \rho_o^o)^{1/2}$: The solid calculated line is based on Eq. (11). (g) $\ln(T_c)$ versus $(A - A_o)^{-1/2}$. The best fit to the linearization of Eq. (10) (see Table I for the fit parameters).

diation of the e-e interaction, V_{ee}^f ,^{6,7} is the driving mechanism behind the surge of each of these features. We illustrate this argument by considering the spin-fluctuation case, as in Ref. 6. There, $I^2\chi(\omega)$ [I is an exchange coupling while $\chi(\omega)$ is a dynamic susceptibility] plays the same role as that of Eliashberg’s electron-phonon spectral function $\alpha^2\mathcal{F}(\omega)$. V_{ee}^{sf} can then be obtained from the integral over frequencies of such an Eliashberg’s type spectral function.

Below, we give a short summary of the main expressions describing $T_c(\ell)$, $A(\ell)$ and their correlations with each other as well as with $\rho_o(\ell)$.

1. Expression of $T_c(\ell)$

Adopting the traditional strategy for calculating $T_c(\ell)$, we solved the set of coupled linearized Eliashberg’s equations within the BCS limit. In this limit, $T_c(\ell)$ is determined by the superconducting coupling constant $\lambda(\ell) = N(\epsilon_F)V_{ee}^{\text{sf}}(\ell) = 2 \int d\omega \frac{I^2\chi(\omega)}{\omega_{\text{opt}}^2 + \omega^2}$, where ω_{opt} is an optimal frequency at which λ is maximal, and can thus be written as:⁴⁷

$$T_c(\ell) = \theta \exp\left(\frac{-1 - \lambda(\ell)}{\lambda(\ell) - \mu^*}\right), \quad (6)$$

where μ^* is the Coulomb pseudopotential and θ is an energy scale that depends on the cut-off bandwidth ω_c^{sf} .

2. Expression of $A(\ell)$

Applying a variational approach to the linearized version of Boltzmann’s transport equations within the relaxation time approximation (wherein the inverse scattering time is calculated by the use of Fermi’s golden rule) we obtain⁴⁷ $\rho(\ell) = A(\ell)T^2$ and

$$A(\ell) = F_\ell^2 \left| \frac{\lambda(\ell) - \mu^*}{1 + \lambda(\ell)} \right|^2. \quad (7)$$

Here, F_ℓ represents the efficiency of momentum relaxation and the availability of phase space for scattering.⁴⁷ Within the FL phase, ℓ is long, $1 \ll k_F\ell_p < \infty$, and ρ_o is small (k_F = Fermi wave number); as such, Eq. (7) can be expanded around $\lambda_o = \lambda(\ell \rightarrow \infty)$ of the normal matrix as

$$A(\ell) \simeq a_o + a_1(\delta\lambda) + a_2(\delta\lambda)^2 + \mathcal{O}[(\delta\lambda)^3], \quad (8)$$

wherein $a_o = A(\ell \rightarrow \infty) = \frac{|\lambda_o - \mu^*|^2}{1 + \lambda_o}$ refer to the negligibly small kinematically-constrained non-fluctuating contributions; the second and third term [containing $\delta\lambda = \lambda(\ell) - \lambda_o$ and the coefficients $a_1 = 2F_\ell^2(|\lambda_o - \mu^*|(1 + \mu^*)/(1 + \lambda_o)^3$ and $a_2 = F_\ell^2(1 + \mu^* - 2|\lambda_o - \mu^*|)(1 + \mu^*)/(1 + \lambda_o)^4$] denote contributions from all kinematically unconstrained relaxation processes after incorporating the fluctuation-mediated channel.

The second-order polynomial expression of $A(\ell)$, Eq. 8, is reminiscent of the empirical *quadratic-in- ρ_o* of Eq. 4.

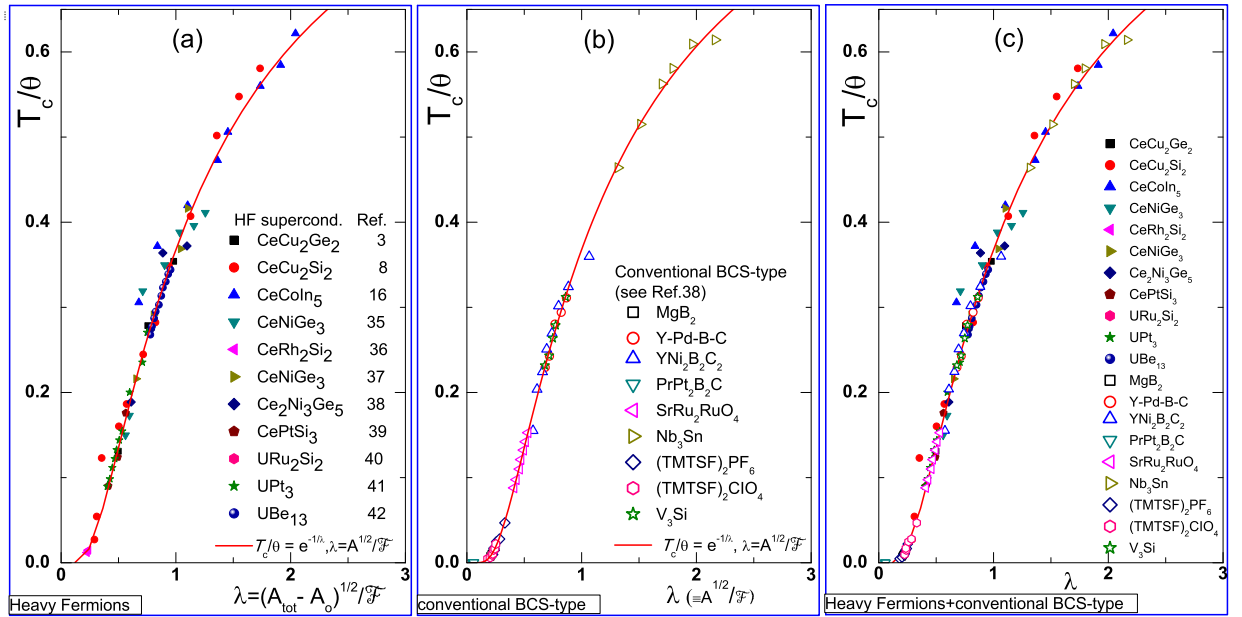


FIG. 5. (a) The generalized plot of $\frac{T_c(p)}{\theta}$ versus $\lambda = \frac{(A-A_0)^{\frac{1}{2}}}{\mathcal{F}}$ of the tabulated HF superconductors.^{3,8,16,25,35-42} (b) For comparison, we include the plot of the same relation in conventional superconductors (data taken from Ref. [43]). (c) A collapse of data from all HF and conventional superconductors on the single $T_c/\theta = \exp(-1/\lambda)$ curve: an unsurprising result considering panels (b) and (c); nevertheless, considering the diversity of the superconducting materials, this plot is highly nontrivial. Each pair of sample-dependent θ and \mathcal{F} was evaluated within the pressure range wherein Eq. (10) is valid [see Figs. 2(g), 3(g), and 4(g)]. Representative values of θ and \mathcal{F} are shown in Table I. As evident, the distribution region of the pairs $(T_c/\theta, \lambda)$ in both HF and strong-coupled superconductors are similar, with the upper limit being $\approx (0.6, 2.1)$ (for λ limit of strong superconductors, see Ref. 20 and also Fig. 4 of Ref. 43). As mentioned for CeCu_2X_2 and CeCoIn_5 , λ is corrected using $\frac{(A-A_0)^{\frac{1}{2}}}{\mathcal{F}}$. Similar plot, but with no $\frac{(A-A_0)^{\frac{1}{2}}}{\mathcal{F}}$ correction, was reported for both pnictide and chalcogenides superconductors.^{44,45} Finally, it is emphasized that the relatively high values of $\frac{T_c(p)}{\theta}$ (those close to 1) should not be substituted in Eq. 14 since this equation is valid only within the $\frac{T_c}{\theta} \ll 1$ condition.⁴⁶

Below we look for an analytical description of $A(\rho_0)$. Let us start by recalling that, in a typical Fermi liquid, the frequency dependence of the imaginary part of the self energy is given by $\text{Im}\Sigma(\omega) \sim \omega^2$. Then, on considering the relevant energy scale to be set by $k_B T$, one obtains the characteristic FL *quadratic-in-T* resistivity. Intuitively, this is related to the fact that, for a given temperature T , $N(E_F)k_B T$ single particles within the Fermi surface are participating in the fluctuation-mediated two-particle channel (each single particle can scatter into one another via this fluctuation-mediated scattering process): this generates the well-known AT^2 resistivity contribution. Specifically, our analysis showed that this channel leads to a FL state with A as in Eq. 7 and superconductivity with T_c as in Eq. 6. Moreover, at $T = 0$ limit, the relevant energy scale is set by the *fuzziness* of the Fermi surface which is determined by δg . Just as the case for the ω^2 -leading-to- T^2 -contribution, we expect $\rho_0 \propto \delta\lambda \propto (\delta g)^2$.⁵⁵ This allows us to establish a correlation among ρ_0 and each of T_c and A (each is a function of ℓ). Guided by these considerations, as well as the empirical relation of Eq. 4, we consider

$$A(\ell) \simeq A_0 + A_1(\rho_0) + A_2(\rho_0)^2, \quad (9)$$

where A_i ($i = 0, 1, 2$) are functions of F_ℓ^2 , μ^* , and λ_0 . Eq. 9 suggests three limiting contributions to $A(\ell)$: (i) The host contribution (dominant $A_0 \neq 0$ when $A_1 \approx 0$ and $A_2 \approx 0$); (ii) a single-particle-like Koshino-Taylor-type ($A - A_0$) $\propto \rho_0$, contribution (dominant $A_1 \neq 0$ contribution); and (iii) an $(A - A_0) \propto (\rho_0)^2$ contribution (a dominant A_2 and a negligible A_1). Results of Figs. 2(e), 3(e), 4(e) belong to the third case.

3. Correlation between $T_c(\ell)$ and $A(\ell)$

Combining the expressions for $T_c(\ell)$ in Eq. 6 and $A(\ell)$ in Eq. 7, we arrive at:

$$T_c(\ell) = \theta e^{-\mathcal{F}/\sqrt{A(\ell)}}. \quad (10)$$

This universal and exact kinematic scaling relation (valid for long ℓ , low ρ_0 : the Fermi-liquid region) is the essence of the relations of Eq. (5) and Figs. 2(g), 3(g), and 4(g). Eq. (10) is most remarkably manifested in Fig. 5: an increase (decrease) of pressure leads to a downwards (upwards) flow of $T_c(\ell)$ towards weaker (stronger) couplings, without ever leaving the curve given by Eq. (10).

Finally, a simplified but approximate relation between T_c and $(\rho_o - \rho_o^\circ)$ can be obtained in the specific case wherein the *quadratic-in- ρ_o* term in Eq. 9 is dominant. Substituting Eqs. (4 and 7) into Eq. 10, we obtain

$$T_c(\ell) \approx \theta \exp\left(\frac{-\mathcal{F}}{\sqrt{A_2}[\rho_o(\ell) - \rho_o^\circ]}\right) \quad (11)$$

On substituting θ , \mathcal{F} , A_2 , and ρ_o° of Table I into this equation, one obtains the solid curves of Figs. 2(f), 3(f), 4(f); this excellent description of experimental data with no fitting parameters is no surprise since, as mentioned above, Eq. (11) is a derived one.

III. Discussion and Conclusions

The similarity of the phase diagrams shown in Figs. 2,3,4, as well as those of other HF superconductors,^{1,2} suggests a generalized T - p phase diagram that highlights the similarity in the cascade of distinct electronic states and in the overall evolution of $T_c(\ell)$, $A(\ell)$, and $\rho_o(\ell)$. Of particular interest to this work is the nontrivial manifestation, in all phase diagrams, of a superconductivity, a FL character and their correlations (see Figs. 2, 3, 4, and 5). We argue above that the surge of all these features and correlations is driven by the spin-fluctuation/valence-fluctuation mediated e-e channel operating within the FL range of the studied HF superconductors.⁵⁶

It happened that for these fluctuations to be well defined quasiparticles and for the Migdal-Eliashberg theoretical framework to be applicable, one needs to ensure that ℓ is long which for the spin-fluctuation case translates into $\chi(\omega)$ and V_{ee}^{sf} being weak and, as a consequence, reduced ρ_o , A , and T_c . In fact this argument, turned around, can be used to define the FL range which can be reached by an application of higher pressure (see Figs. 2-4), strong magnetic field,³¹⁻³³ or incorporation of non-magnetic impurities:⁵⁷⁻⁶⁰ All promote the weakening of the fluctuation-mediated scattering process.

Based on these arguments, the following inferences can be drawn: First, Figs. 2-4 indicate that on moving out of the FL region but towards the quantum critical points, one observes a continuous enhancement in ρ_o , A , and T_c . This continuity is suggestive of a similarity in the scattering interaction, the strength of which is enhanced on reducing the pressure. However, Figs. 2-4 also indicate that below the FL region our analytical expressions do not reproduce the observed baric evolution of A or T_c . This shortcoming is related to the breakdown of the long- ℓ condition. Nevertheless, this does not invalidate our analysis within the FL region. It is worth repeating that the availability of a FL state is not a precondition for the applicability of our approach. Rather, the surge of the e-e scattering channel gives rise to the FL state, the superconductivity and their correlation.

Second, it was reported that an application of a magnetic field ($H > H_2$) within the superconducting dome of

CeCoIn₅ leads to a quench of superconductivity in favor of a FL normal-state.³¹⁻³³ We attribute this field-induced FL character within the NFL region to a field-induced weakening of the strength of the spin-fluctuation and as such to an increase in ℓ , in reminiscence of the aforementioned increase in applied pressure or in the incorporation of nonmagnetic impurities. Further analysis is underway.

Third, we argued above that within the long- ℓ region, the spin-fluctuation/valence-fluctuation modes are mediating the e-e interaction and this in turn leads to the scaling between $\frac{T_c}{\theta}$ and $(A_{tot} - A_o)$ (see Fig. 5(a)). This is similar to the emergent phonon-mediated scaling reported for other non-HF superconductors: Fig. 5(b) demonstrates the scaling in conventional superconductors.^{43,47} Similar scaling was reported for the Fe-based pnictides⁴⁴ and chalcogenides.⁴⁵ Although the superconductivity in these series are considered to be driven by spin-fluctuation mediated pairing¹⁰ however we did not include these Fe-based materials in Fig.5 since these reports did not include a correction for the non-fluctuation-related contribution: A_{tot} was used instead of $(A_{tot} - A_o)$.

We extend our present analysis by including a discussion⁴⁷ of two specific parameters of the HF superconductors: (i) the Kadowaki-Woods ratio and (ii) the gap-to- T_c ratio. We show that the influence of the fluctuation processes on both ratios can be accounted for by including an additional factor which embodies the material properties of these HF superconductors.

(i) Jacko *et al.*⁶¹ accounted for the wide difference among the Kadowaki-Woods ratio of a variety of strongly coupled systems by demonstrating that

$$\frac{A}{\gamma^2} = \left(\frac{81}{4\pi\hbar k_B^2 e^2}\right) \left(\frac{1}{d^2 n N^2(\epsilon_F) \langle v_{0x}^2 \rangle}\right) = (f_{con}) \left(\frac{1}{f_{mat}}\right), \quad (12)$$

wherein $\langle v_{0x}^2 \rangle$ is an average of the carrier velocity squared (a measure of the anisotropies), n is the carrier density, $N(\epsilon_F)$ is the density of states at the Fermi level, and $d \sim 1$ is a dimensionless number. Apparently, due to the material-dependent second factor, $\frac{A}{\gamma^2}$ of Eq. 12 is nonuniversal. This shortcoming would be most evident for the ratio of the fluctuation-bearing HF superconductors within their Fermi-liquid region (see Figs. 2-4). Our evaluation of the Kadowaki-Woods ratio (Eq. 12) of these HF superconductors gives

$$\frac{A}{\gamma^2} = \left(\frac{81}{4\pi\hbar k_B^2 e^2}\right) \left(\frac{F_\ell}{d^2 n N^2(\epsilon_F) \langle v_{0x}^2 \rangle}\right) = (f_{con}) \left(\frac{F_\ell}{f_{mat}}\right), \quad (13)$$

wherein the material-dependent F_ℓ factor is as described in Eq. (7). It is not close to 1 as assumed during the derivation of Eq. (12).⁶¹ Rather $F_\ell > 1$: a larger *apparent* ratio because of the easing of the kinematic constraints in these fluctuation-bearing systems. As in Ref. 61, the

universal character is restored only when expressed as

$$\frac{A}{\gamma^2} \left(\frac{f_{\text{mat}}}{F_\ell} \right) = \frac{A \cdot f'_{\text{mat}}}{\gamma^2} = f_{\text{con}}.$$

(ii) Carbotte⁴⁶ derived an approximate expression for the gap-to- T_c ratio of strong-coupled superconductor. Modified to the case of a fluctuation-bearing superconductor within $\frac{T_c}{\theta} \ll 1$ region, this expression reads as

$$\frac{2\Delta(\ell)}{k_B T_c(\ell)} \approx 3.53 \left\{ 1 + 12.5 \left[\frac{T_c(\ell)}{\theta} \right]^2 \ln \left[\frac{\theta}{2T_c(\ell)} \right] \right\}, \quad (14a)$$

$$\approx 3.53 \left\{ 1 + 12.5 \left[e^{-\mathcal{F}/\sqrt{A(\ell)}} \right]^2 \ln \left[\frac{1}{2e^{-\mathcal{F}/\sqrt{A(\ell)}}} \right] \right\} \quad (14b)$$

Thus, within $\frac{T_c}{\theta} \ll 1$ region, the gap-to- T_c ratio can be fine-tuned: From $2\Delta(\ell \rightarrow \infty)/k_B T_c(\ell \rightarrow \infty) = 3.53$, the universal BCS value, up to a higher nonuniversal value by varying the control-parameter that modifies ℓ .

Finally, it is worth adding that our internally-consistent empirical and theoretical analyses are based on a clear identification of the difference between the fluctuation-related and normal (non-fluctuation-related) contributions within the fluctuation-related FL region (which starts when the resistivity manifests the T^2 contribution and ends when $T_c \rightarrow 0$).

In summary, we investigated the superconductivity, the FL transport, and their correlations within the FL region of the T - p phase diagram of representative quantum-critical HF superconductors. Empirically, on varying the control parameters, (i) the normal-state resistivities manifest the characteristic FL, $\rho_o + AT^2$, character with $A \propto \rho_o^2$ and (ii) the superconducting state manifests a correlation of T_c with A ($\ln \frac{T_c}{\theta} \propto A^{-\frac{1}{2}}$). We attribute the surge of these superconducting and FL transport features and their correlations to a fluctuation-mediated e-e scattering channel. Theoretically, on adopting many-body

techniques, we derive analytic expressions for $T_c(\rho_o)$ and $A(\rho_o)$ and their correlations that reproduce satisfactorily the aforementioned empirical correlations.

Methods

We analyzed the extensively reported pressure-dependent resistivities of various HF superconductors. Within the FL region, we looked for any correlation among the superconductivity (as measured by T_c), the Fermi-liquid character (as measured by A), and the excess in the residual resistivity (ρ_o as a measure of the strength of the scattering channel) when the control parameter is varied. Using graphical and analytical procedures, we managed to identify the empirical expression discussed in Subsec. II B. More importantly, we managed to identify the spin-fluctuation/valence-fluctuation mediated e-e scattering channel as being the driving mechanism behind these correlations. Guided by the inferences drawn from the empirical expressions and the identified channel, we formulated the theoretical framework outlined in Subsec. II B and Sec. II C: Basically, we started with the spin-fluctuation/valence-fluctuation exchange mechanism which is different from the traditional mechanisms in that it takes into consideration the modification in the kinematic constraints which, in turn, lead to a significant enlargement in the phase space available for scattering. Then, after applying the standard theories of Migdal-Eliashberg (superconductivity) and Boltzmann (transport), we managed to derive the analytic expressions of Subsec. II B which satisfactorily explain the empirical observations.

Acknowledgments

We acknowledge partial financial support from Brazilian agency CNPq.

* massalam@if.ufrj.br

† CASTRO.Pedro@nims.go.jp

‡ mbsn@if.ufrj.br

¹ P. Gegenwart, Q. Si, and F. Steglich, *Nat. Phys.* **4**, 186 (2008).

² P. Coleman, *Handbook of Magnetism and Advanced Magnetic Materials* (2007).

³ D. Jaccard, H. Wilhelm, K. Alami-Yadri, and E. Vargoz, *Physica B* **259-261**, 1 (1999).

⁴ H. Q. Yuan, F. M. Grosche, M. Deppe, C. Geibel, G. Sparn, and F. Steglich, *Science* **302**, 2104 (2003).

⁵ H. v. Löhneysen, A. Rosch, M. Vojta, and P. Wölfle, *Rev. Mod. Phys.* **79**, 1015 (2007).

⁶ N. D. Mathur, F. M. Grosche, S. R. Julian, I. R. Walker, D. M. Freye, R. K. W. Haselwimmer, and G. G. Lonzarich, *Nature* **394**, 39 (1998).

⁷ K. Miyake and S. Watanabe, *Philos. Mag.* **97**, 3495 (2017).

⁸ A. T. Holmes, D. Jaccard, and K. Miyake, *Phys. Rev. B* **69**, 024508 (2004).

⁹ D. Pines, *J. Phys. Chem. B* **117**, 13145 (2013).

¹⁰ D. J. Scalapino, *Reviews of Modern Physics* **84**, 1383 (2012).

¹¹ T. A. Maier, S. Karakuzu, and D. J. Scalapino, *Phys. Rev. Research* **2**, 033132 (2020).

¹² Z. Li, S. Kivelson, and D. Lee, *npj Quantum Mater* **6**, 36 (2021).

¹³ M. Dean, G. Dellea, R. S. Springell, F. Yakhou-Harris, K. Kummer, N. Brookes, X. Liu, Y. Sun, J. Strle, T. Schmitt, *et al.*, *Nature materials* **12**, 1019 (2013).

¹⁴ N. Lee-Hone, H. Özdemir, V. Mishra, D. Broun, and P. Hirschfeld, *Phys. Rev. Res.* **2**, 013228 (2020).

- ¹⁵ N. Lee-Hone, J. Dodge, and D. Broun, Phys. Rev. B **96**, 024501 (2017).
- ¹⁶ V. Sidorov, M. Nicklas, P. Pagliuso, J. Sarrao, Y. Bang, A. V. Balatsky, and J. D. Thompson, Phys. Rev. Lett. **89**, 157004 (2002).
- ¹⁷ The assumption of a formation of a patch within which quantum critical fluctuations emerge does not contradict the requirement that quantum critical fluctuations are scale invariant and extend over a large-sized region. This is because the length scale of each patch is taken to be longer than the mean free path and coherence length. This assumption is invoked for taking care of the excess residual resistivity and its usefulness in reconciling the influence from each of disorder, pressure or magnetic field. Within each patch, $\delta\mathbf{g} \neq 0$.
- ¹⁸ G. Bergmann, Phys. Rev. B **3**, 3797 (1971).
- ¹⁹ G. Bergmann, Phys. Rep. **27**, 159 (1976).
- ²⁰ M. Gurvitch, Phys. Rev. Lett. **56**, 647 (1986).
- ²¹ In cases where $X_c^o \approx 0$, one considers $X \approx X_{tot}$.
- ²² An incorporation of nonmagnetic impurities⁵⁷⁻⁶⁰ leads to a reduction in $\chi(\omega)$ and V_{ee}^{st} and, as a consequence, to a drop in both A and T_c .
- ²³ A. Rosch, Phys. Rev. Lett. **82**, 4280 (1999).
- ²⁴ S. Kambe and J. Flouquet, Solid State Commun. **103**, 551 (1997).
- ²⁵ I. Sheikin, D. Braithwaite, J.-P. Brison, W. Assmus, and J. Flouquet, J. Low Temp. Phys. **118**, 113 (2000).
- ²⁶ P. Gegenwart, C. Langhammer, C. Geibel, R. Helfrich, M. Lang, G. Sparn, F. Steglich, R. Horn, L. Donnevert, A. Link, and W. Assmus, Phys. Rev. Lett. **81**, 1501 (1998).
- ²⁷ F. Honda, T. Maeta, Y. Hirose, Y. Onuki, A. Miyake, and R. Settai, J. Korean Phys. Soc. **63**, 345 (2013).
- ²⁸ B. Bellarbi, A. Benoit, D. Jaccard, J. M. Mignot, and H. F. Braun, Phys. Rev. B **30**, 1182 (1984).
- ²⁹ J.-P. Rueff, S. Raymond, M. Taguchi, M. Sikora, J.-P. Itié, F. Baudelet, D. Braithwaite, G. Knebel, and D. Jaccard, Phys. Rev. Lett. **106**, 186405 (2011).
- ³⁰ E. Miranda and V. Dobrosavljević, Rep. on Prog. in Phys. **68**, 2337 (2005).
- ³¹ J. Paglione, M. A. Tanatar, D. G. Hawthorn, E. Boaknin, R. W. Hill, F. Ronning, M. Sutherland, L. Taillefer, C. Petrovic, and P. C. Canfield, Phys. Rev. Lett. **91**, 246405 (2003).
- ³² A. Bianchi, R. Movshovich, I. Vekhter, P. G. Pagliuso, and J. L. Sarrao, Phys. Rev. Lett. **91**, 257001 (2003).
- ³³ E. D. Bauer, C. Capan, F. Ronning, R. Movshovich, J. D. Thompson, and J. L. Sarrao, Phys. Rev. Lett. **94**, 047001 (2005).
- ³⁴ F. Ronning, C. Capan, E. D. Bauer, J. D. Thompson, J. L. Sarrao, and R. Movshovich, Phys. Rev. B **73**, 064519 (2006).
- ³⁵ H. Kotegawa, K. Takeda, T. Miyoshi, S. Fukushima, H. Hidaka, T. C. Kobayashi, T. Akazawa, Y. Ohishi, M. Nakashima, A. Thamizhavel, *et al.*, J. Phys. Soc. Jpn. **75**, 044713 (2006).
- ³⁶ S. Araki, M. Nakashima, R. Settai, T. C. Kobayashi, and Y. Onuki, J. Phys.: Condens. Matter **14**, L377 (2002).
- ³⁷ M. Nakashima, K. Tabata, A. Thamizhavel, T. C. Kobayashi, M. Hedo, Y. Uwatoko, K. Shimizu, R. Settai, and Y. Onuki, J. Phys.: Condens. Matter **16**, L255 (2004).
- ³⁸ M. Nakashima, H. Kohara, A. Thamizhavel, T. D. Matsuda, Y. Haga, M. Hedo, Y. Uwatoko, R. Settai, and Y. Onuki, Physica B: Cond Matter **378**, 402 (2006).
- ³⁹ Y. Onuki, Y. Miyauchi, M. Tsujino, Y. Ida, R. Settai, T. Takeuchi, N. Tateiwa, T. D. Matsuda, Y. Haga, and H. Harima, J. Phys. Soc. Jpn. **77**, 37 (2008).
- ⁴⁰ E. Hassinger, G. Knebel, K. Izawa, P. Lejay, B. Salce, and J. Flouquet, Phys. Rev. B **77**, 115117 (2008).
- ⁴¹ A. de Visser, J. Franse, and A. Menovsky, J. Magn. Magn. Mater. **43**, 43 (1984).
- ⁴² H. R. Ott, H. Rudigier, Z. Fisk, and J. L. Smith, Phys. Rev. Lett. **50**, 1595 (1983).
- ⁴³ M. Nunez-Regueiro, G. Garbarino, and M. D. Nunez-Regueiro, J Phys: Conf Series **400**, 022085 (2012).
- ⁴⁴ P. B. Castro, J. L. Ferreira, M. B. S. Neto, and M. El-Massalami, J. Phys.: Conf. Ser. **969**, 012050 (2018).
- ⁴⁵ C. Soares, M. ElMassalami, Y. Yanagisawa, M. Tanaka, H. Takeya, and Y. Takano, Sci. Rep. **8**, 7041 (2018).
- ⁴⁶ J. P. Carbotte, Rev. Mod. Phys. **62**, 1027 (1990).
- ⁴⁷ M. ElMassalami and M. B. S. Neto, Phys. Rev. B **104**, 014520 (2021).
- ⁴⁸ W. E. Lawrence and J. W. Wilkins, Phys. Rev. B **7**, 2317 (1973).
- ⁴⁹ W. E. Lawrence, Phys. Rev. B **13**, 5316 (1976).
- ⁵⁰ A. H. MacDonald, Phys. Rev. Lett. **44**, 489 (1980).
- ⁵¹ A. H. MacDonald, R. Taylor, and D. J. W. Geldart, Phys. Rev. B **23**, 2718 (1981).
- ⁵² B. Patton and A. Zaringhalam, Phys. Lett. A **55**, 95 (1975).
- ⁵³ C. J. Pethick, D. Pines, K. F. Quader, K. S. Bedell, and G. E. Brown, Phys. Rev. Lett. **57**, 1955 (1986).
- ⁵⁴ (), see Ref. 47 for a discussion on the two reported exceptions.
- ⁵⁵ (), based on Eq. (5) of Ref. 62, for low defects, one obtains $\delta\lambda_\ell \propto \frac{1}{\ell} \propto \rho_o$.
- ⁵⁶ (), such an argument, supported by the aforementioned agreement between theory and experiments, is not in contradiction with the fact that there are difference in the details of the corresponding phase diagrams (e.g. the number and type of T_c -domes, the number and type of the critical/crossover points p_m , p_v , etc.): In fact, irrespective of these details, all studied phase diagrams manifest quantum critical instabilities which are accompanied by critical spin-fluctuations⁶ or valence-fluctuations^{7,8}.
- ⁵⁷ J. L. Smith, Z. Fisk, J. O. Willis, B. Batlogg, and H. R. Ott, J Appl Phys **55**, 1996 (1984).
- ⁵⁸ G. Adrian and G. Saemann-Ischenko, Zeitschrift für Physik B Condensed Matter **72**, 235 (1988).
- ⁵⁹ G. Adrian and H. Adrian, Physica C: Superconductivity **153-155**, 435 (1988).
- ⁶⁰ G. Adrian and H. Adrian, J Less Common Met **149**, 313 (1989).
- ⁶¹ A. C. Jacko, J. O. Fjærestad, and B. J. Powell, Nat Phys **5**, 422 (2009).
- ⁶² G. Bergmann, Z. Physik **228**, 25 (1969).